Translationally invariant metamirrors for spatial filtering of light beams

P. Y. Wang,[1,*] R. Herrero,[2] M. Botey,[2] Y. C. Cheng,[1] and K. Staliunas[2,3,4]
[1]*Department of Electro-Optical Engineering, National Taipei University of Technology (NTUT), No.1, Sec. 3, Zhongxiao E. Rd., Da'an Dist., 10608, Taipei, Taiwan*
[2]*Departament de Fisica i Enginyeria Nuclear, Universitat Politècnica de Catalunya, Colom 11, 08222 Terrassa, Barcelona, Spain*
[3]*Institució Catalana de Recerca i Estudis Avançats (ICREA), Pg. Lluís Companys, 23, 08010 Barcelona, Spain*
[4]*Vilnius University, Laser Research Center, Saulėtekio al. 10, Vilnius, Lithuania*

(Received 22 February 2020; accepted 18 May 2020; published 30 July 2020)

We propose a translationally invariant metamirror for light filtering in reflection. The device consists of a thin transverse grating in the micron scale positioned in front of a flat mirror. We analyze the performance of such a photonic metamirror and find a modification of the angular spectrum of the reflected beams, leading to a significant reduction of the beam divergence for particular configurations. This study points toward a type of optical component, a flat metamirror with a filtering functionality and no alignment requirements, due to its translational invariance.

DOI: 10.1103/PhysRevA.102.013517

I. INTRODUCTION

Efficient spatial (angular) filtering, among others, is a key mechanism for the improvement of the spatial characteristics of laser emission. Typically, conventional lasers (e.g., solid-state lasers) contain intracavity spatial filters in the form of confocal arrangements of lenses with a filtering diaphragm at the focal plane to modify the far-field intensity profile. This ensures the emission of the laser on the lowest transverse (Gauss-Hermite, or Gauss-Laguerre) mode with maximum brightness of emission, as most of the pump energy converts into the lowest order mode.

Apart from the above described confocal lens spatial filtering arrangement, other methods have been proposed, mostly based on external gratings or external feedback schemes [1–4]. These alternative methods, however, did not result in broad practical applications, for their low efficiency, and for inconveniences due to their relatively large size and precise alignment requirements. An alternative method for spatial filtering based on the photonic crystals (PhCs) was recently proposed and developed [5–13]. The method was first demonstrated in a single transmission scheme, later was applied for intracavity filtering arrangements in microchip [14] and semiconductor [15] microlasers, and increased the brightness of the radiation increased several times. However, the efficient fabrication of such PhCs spatial filters is technically challenging, due to requirement that the filtering PhCs must be at least two-dimensional (2D): one periodic modulation component along the light propagation (longitudinal) direction, and another in a transverse direction. Therefore, at least 2D PhCs are required to provide a 1D spatial filtering effect (cylindrical filtering), and, respectively, 3D PhCs are necessary for 2D filtering (axisymmetric filtering [16]). The fabrication of such structures, with sufficient refractive index contrast, represents a real challenge for technology today. Up to now, experimental demonstration of PhCs spatial filtering has only been achieved with structures fabricated by direct laser writing technologies, with perhaps a single exception, where layer by layer atomic vaporization technique was applied [17].

An ideal filtering optical component would thereby be a thin and flat spatial filter: Not only for its use (the thickness is crucial for an intracavity use in microlasers), but also for fabrication convenience. Usually, the fabrication of 2D flat structures is less challenging than of 3D volumetric structures: several efficient technologies were developed for the manufacturing of flat structures (lithographic or vaporization techniques [18–21]). However, from a conventional understanding of the physics of PhCs spatial filtering, the longitudinal modulation is necessary for spatial filtering as well. Therefore, a compromise situation, combining the advantages of the flat optics and 2D/3D PhCs filtering, would be a thin grating positioned parallel and close to the surface of a mirror. Such an arrangement is equivalent to two gratings, the real one and the mirror-image one, separated by twice the distance to the mirror surface [see Fig. 1(a)]. When the grating is mainly supposed to transmit (if reflection is not relevant) the theoretical treatment is extremely simple, as it considers double forward diffraction from such gratings. This is the case for low-contrast gratings, relatively smooth photonic structures. However, when back-reflections are relevant, for gratings with larger index contrast, the flat metamirror arrangement must be treated as a Fabry-Perot (FP) resonator. In this latter case, the structured metamirror induces various intertwined optical effects, as scattering from the grating, interferences from the FP cavity, and Mie resonances from the individual elements composing the grating, and the analytical treatment becomes complicated.

The above considerations bring us to an intuitive idea, that, if the grating is positioned close and parallel to the mirror surface, it can hold some of the features of a 3D PhC spatial filter. In fact, the application of compact gratings with spatial

*peggy831110pp@gmail.com

 ©2020 American Physical Society

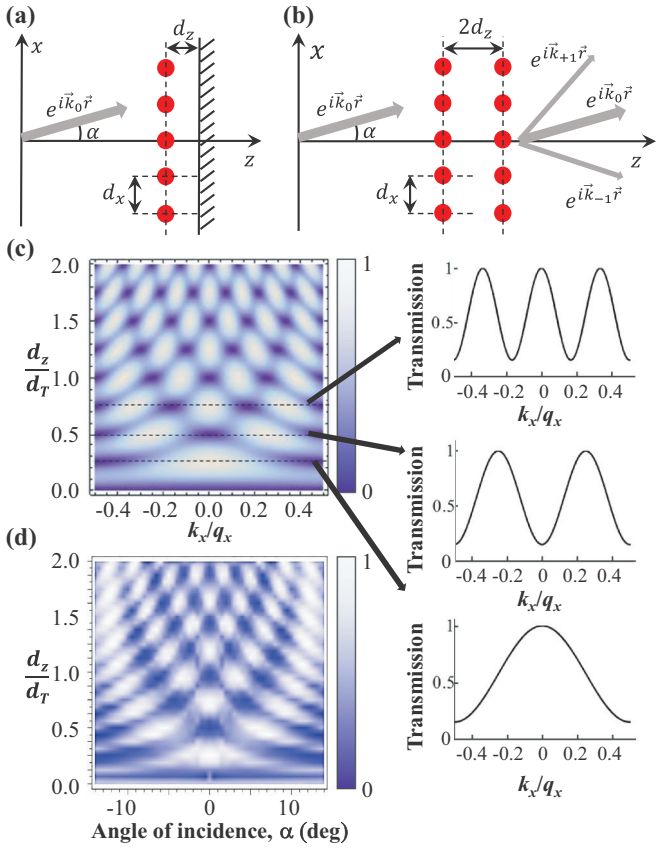

FIG. 1. Scheme and the filtering maps. A diffraction grating positioned in front- and parallel to a mirror at a distance d_z (a), is equivalent to two gratings, the real- and the mirror-image one, separated by distance $2d_z$, as shown in (b). (c) Zero-diffraction-order transmission coefficient (corresponding to zero-order reflection in the original metamirror configuration) in (k_x, d_z) parameter space, for $s = 0.5$. Cross sections show the angular transmission lines for multiples of 1/4 of the Talbot distance, $d_T = 4\pi k_0/q_x^2$ (d) FDTD calculated transmission map (supercell FDTD-2D calculation), in the parameter space of (α , d_z), for comparison, for a structure made of an array of circles of diameter equals to 0.8 μm and a refractive index of 1.2 embedded in air, $d_x = 2$ μm, $\lambda = 1$ μm, and with corresponding Talbot distance of 8 μm.

filtering performance have been proposed for microlasers [22] or as a spatial filter in telecom wavelength range [23]. However, a comprehensive theoretical model for the explanation of the filtering properties—the depth and the width of the angular filtering dips, the efficiency of filtering—remains an open question. The present work explores the proposed idea by modeling the described photonic structure under different approximations. We start from a simplified paraxial model, valid for low refraction index contrast structures, which allows explicit analytical estimations, as presented in Sec. II. This approach accounts for only forward-diffraction from the grating. We continue with more precise semianalytical model, valid for high contrast structures, analogous to transversally structured FP resonators, in Sec. III. The analysis also provides quasianalytical estimations that uncover additional effects, such as FP effects and Mie resonances of the scatterers. Both analytical and quasianalytical models are verified by the finite difference time domain (FDTD) simulations performed in RSoft commercial software, using supercell techniques also a direct FDTD calculations in a large transverse domain. The main result of the present article is a demonstration that the proposed planar and translationally invariant metamirrors show spatial filtering effects and offer a technologically relevant platform to improve the performance of microlasers.

II. LOW INDEX CONTRAST MODEL (FORWARD DIFFRACTION MODEL)

First, we consider a structured layer with a low refraction index contrast as sketched in Fig. 1: a grating at a distance d_z from a 100% reflecting mirror [Fig. 1(a)], which is equivalent to the unfolded structure consisting of two identical gratings (real and mirror-image) separated by a distance of $2d_z$ [Fig. 1(b)]. We assume a simplification of the scheme by neglecting the back-diffraction from the gratings. Indeed, when the scattering by gratings is weak, $s \ll 1$ (scattering in terms of intensity is s^2), the back-reflections contribution is negligible. This also occurs when the gratings is smooth along the propagation direction, which is the case for instance, in laser-writing fabrication [19], where the index modifications are elongated voxels. Besides, we only take into account the first diffraction orders, as the higher diffraction orders may also be neglected for small scattering efficiency as well as for submicrometer transverse periods.

A plane wave with wave vector $\vec{k}_0$ incident at angle α onto the grating is $\vec{k}_0 = (k_x, k_z)$, where $k_x = |\vec{k}_0|\sin(\alpha)$ and $k_z = |\vec{k}_0|\cos(\alpha)$, respectively. The forward scattering from the grating with transverse period d_x results in three relevant diffracted beam components with respective transverse wave vectors: $k_x - q_x$, k_x, $k_x + q_x$ being $q_x = 2\pi/d_x$ the wave number of the modulation along the x axis. These field amplitude components may be written in the form of a column vector $\vec{A} = (A_{-1}, A_0, A_{+1})^T$ (T means transpose), which is transformed by the grating transmission matrix (see Appendix A):

$$\hat{S} = \begin{bmatrix} \frac{\cos(\sqrt{2}s)+1}{2} & \frac{i\sin(\sqrt{2}s)}{\sqrt{2}} & \frac{\cos(\sqrt{2}s)-1}{2} \\ \frac{i\sin(\sqrt{2}s)}{\sqrt{2}} & \cos(\sqrt{2}s) & \frac{i\sin(\sqrt{2}s)}{\sqrt{2}} \\ \frac{\cos(\sqrt{2}s)-1}{2} & \frac{i\sin(\sqrt{2}s)}{\sqrt{2}} & \frac{\cos(\sqrt{2}s)+1}{2} \end{bmatrix}. \quad (1)$$

The matrix (1) is unitary, to ensure the energy conservation, and that s stands for the scattering of the grating in terms of the amplitude. The full amplitude of the transmitted field is

$$A(\vec{r}) = A_0 e^{i\vec{k}_0\cdot\vec{r}} + A_{-1}e^{i(\vec{k}_0-\vec{q})\cdot\vec{r}} + A_{+1}e^{i(\vec{k}_0+\vec{q})\cdot\vec{r}} \quad (2)$$

under the first diffraction order approximation. The free propagation in space between the gratings is described by the diagonal propagation matrix, $\hat{P}$:

$$\hat{P} = \mathrm{Diag}\left(e^{\frac{-i(k_x-q_x)^2 d_z}{k_0}}, e^{\frac{-ik_x^2 d_z}{k_0}}, e^{\frac{-i(k_x+q_x)^2 d_z}{k_0}}\right), \quad (3)$$

as follows from the paraxial propagation model (see Appendix A).

The total transmission matrix through the double-grating arrangement is $\hat{T} = \hat{S}\hat{P}\hat{S}$. The element of the transmission matrix T_{22}, determines the transmission of the central, k_0 component (corresponds to reflection in the original

arrangement):

$$T_{22} = \left(\cos^2(\sqrt{2}s) - e^{\frac{-id_z q_x^2}{k_0}} \sin^2(\sqrt{2}s) \cos\left(\frac{2k_x q_x d_z}{k_0}\right)\right) e^{\frac{-id_z k_x^2}{k_0}}. \tag{4}$$

Figure 1(d) presents the FDTD calculations results from the Eq. (4) of zero-order transmission. Note that Eq. (4) allows simple, analytically tractable estimations of the characteristic of angular filtering performance of the proposed metamirror.

The result is that the transmission coefficient is periodic with respect to the incidence angle, whereas the dependence on the distance between the grating and mirror is more complicated. For instance, the amplitude of the transmission of the on-axis plane wave component is periodic with the distance:

$$|T_{22}| = \left(\cos^2(\sqrt{2}s) - e^{\frac{-id_z q_x^2}{k_0}} \sin^2(\sqrt{2}s)\right), \tag{5}$$

as follows from Eq. (4). The periodicity, however, does not hold for every angle. At normal incidence, the structure is transparent $|T_{22}| = 1$ for grating-mirror distances: $d_z q_x^2/k_0 = \pi(1 + 2m)$, (where m is an integer), while the attenuation is maximal for $d_z q_x^2/k_0 = 2\pi m$, down to the value $|T_{22}|_{\min}$:

$$|T_{22}| = \cos(2\sqrt{2}s) \approx 1 - 4s^2 + \ldots. \tag{6}$$

In other words, the zero-order diffraction component is maximally filtered out (low-angle-pass filtering) for distances between the grating and mirrors equal to $d_z = (2m + 1)\pi k_0/q_x^2$. We can rewrite $d_z = (2m + 1)d_T/4$ denoting $d_T = 4\pi k_0/q_x^2 = 2d_x^2/\lambda$, thus we identify d_T as the Talbot length. It is well known that the Talbot length is the field periodicity in the field propagation direction behind a transverse periodic mask (amplitude or phase grating). The amplitude and the phase modulations in the transverse direction periodically interchange along the wave propagation. The optimum low-angle-pass filtering occurs at grating-mirror distances of odd multiples of 1/4 of the Talbot length $d_z = (2m + 1)d_T/4$. On the contrary, the optimum high-angle-pass filtering is obtained at a distance of even multiples of 1/4 the Talbot length $d_z = 2md_T/4$.

The spatial filtering angle $\sin(\alpha) = k_x/|\vec{k}_0|$, follows from the condition,$\cos(2k_x q_x d_z/k_0) = -1$, and results in $k_x = q_x d_T/8d_z$, i.e., it decreases with the distance between grating and mirror. Full 2D FDTD calculations show good correspondence with this analytical expression, see Fig. 1(d). FDTD simulations consider a grating build from identical circular elements. The FDTD 2D calculations are based on the supercell technique with Bloch-periodic transverse boundary conditions. We assume a rectangular unit cell, 2-μm wide, containing the mirror and one circle-shaped dielectric object.

Inspecting Figs. 1(c) and 1(d), we find that while the agreement is good on a large scale in parameter space, the FDTD calculations show additional reflectance modulations (horizontal fringes on a small scale). This fringing is due to the resonance effects, when the back scattering from each grating (the real one and the mirror-image one) are relevant. The simple forward transmission scheme cannot unveil these FP fringes. However, the comparison shows that the real map is soundly described by the low contrast transmission scheme, overlaid by the FP fringes.

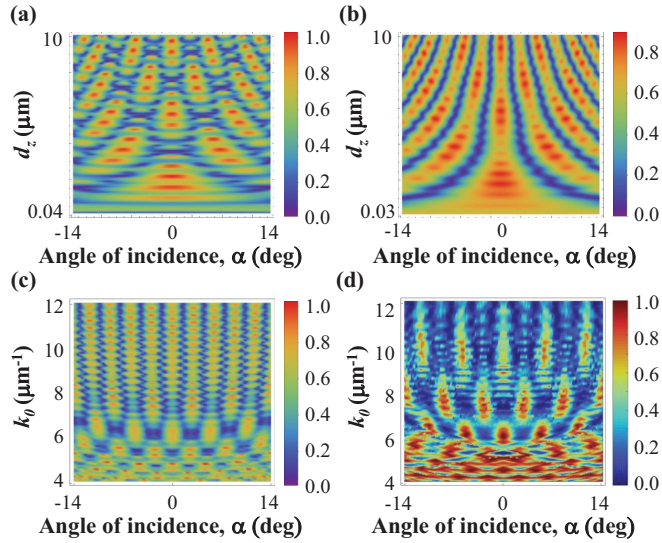

FIG. 2. FP and Mie resonances. Reflectance map calculated by the high index contrast analytical model as a function of the incidence angle and the mirror-grating distance, for rectangular shape scattering objects of different thickness: 0.7 μm (a), and 0.6 μm (b). Width of rectangular scatterers is 1 μm, a transverse period is $d_x = 2\,\mu$m, a refractive index of scatterers is $n_2 = 1.68$ and a distance is $d_z = 9.3$ mm. Reflectance maps for high index contrast from analytical model (c) and numerical FDTD simulation (d). Thickness of the scattering objects 0.3 μm and other parameters the same as in (a).

III. GENERAL MODEL FOR HIGH INDEX CONTRAST

Next, the analytical treatment, including back-diffraction, the FP-cavity effects, and the structure of the grating elements is considered. The grating is now modeled as a layer of equispaced objects, of a given shape and size, in front of high reflection mirror, generating a set of two nested cavities with transverse structure. The reflection matrix of the structured mirror as a function of the incidence angle is

$$\hat{R}_{\text{ref}}(k_x) = [\hat{R} + \hat{T}\hat{P}\hat{R}_M(\hat{I} - \hat{R}\hat{P}\hat{R}_M)^{-1}\hat{T}], \tag{7}$$

where $\hat{R}$ and $\hat{T}$ correspond to the reflection and transmission matrices of the structured layer, respectively, $\hat{I}$ is the identity matrix, $\hat{R}_M$ is the reflection of the mirror, and $\hat{P}$ represents the double propagation between the mirror and grating.

In particular, we consider rectangular scatters and a metallic a 100% reflecting mirror. We use the same field expansion into the zero- and first-diffraction orders, $\vec{A} = (A_{-1}, A_0, A_{+1})^T$, the amplitudes of which are coupled through the diffraction of the structured layer. The derivation of $\hat{R}$ and $\hat{T}$ matrices are provided in Appendix B.

We numerically calculate reflectance maps using this more accurate model as depicted in Fig. 2. The fringed structure of the reflectance maps is associated with the FP resonances due to the cavity between the mirror and the grating, and it is also in good correspondence with the FDTD calculations. The large-scale reflectance modulations of the grating (due to the Talbot effect discussed in the previous section) is now overlaid by the FP resonances. As expected, fringes corresponding to

the FP-like resonances become more pronounced for high index contrasts, compare Figs. 1(d) and 2(a).

On the other hand, the cavity finesse is reduced due to Mie resonances in the individual elements of the grating. The Mie resonances in the individual objects result in the enhancement of the forward scattering and reduction of back scattering, reducing the FP resonances, see Fig. 2(b). The Mie resonances are especially visible when reflectance is scanned as a function of wavelength. In particular, in Fig. 2(c), the cavity fringes disappear for $k_0 = 6\,\mu\text{m}^{-1}$, in agreement with FDTD calculations, see Fig. 2(d).

FDTD 2D supercell simulations consider a plane wave incident at some angle from the normal and a detector placed at the same distance from a totally reflecting mirror. The differences between Figs. 2(c) and 2(d) may be attributed to the fact that transverse resonances are not included in the high index model while they are evidently present in the full FDTD simulations. Anyway, the differences occur far from the interesting filtering regimes. Besides, we have also numerically evaluated (by FDTD) the effect of the scatterer shape (considering circles, ellipses, squares, and rectangles) and found that although unessential differences arise, the main features persist and mainly depend on the refractive index of the scatterers, and on their dimensions.

IV. SPATIAL FILTERING

The analytically calculated angular reflection function, Eq. (3), allows to estimate the spatial filtering efficiency. Starting from a Gaussian initial distribution in the far field, $A_0(k_x)$, the shape of the filtered distribution is calculated by multiplying it by the transmission function as: $A(k_x) = T_{22}(k_x)A_0(k_x)$. We calculate the angular beam width of the filtered distribution as

$$\Delta k^2 = \int \left| A(k_x)^2 k_x^2 dk_x \Big/ \int |A(\mathrm{k}_x)|^2 dk_x \right|, \tag{8}$$

which gives the improvement (reduction) of the beam quality factor, M^2. Calculations do not lead to analytically tractable results, however the numerical study with respect to parameters s and q, uncovers a maximum reduction of the beam quality factor, M^2 by a factor of 2, in an ideal case.

The same analysis was performed numerically. The high index contrast model provides the angular reflection function of the central mode, as shown in Fig. 3(a). The full reflection function multiplied by the angular distribution of the incident Gaussian beam of a given width, is shown in Fig. 3(b). The angular divergence of filtered radiation versus that of the initial radiation, noted as BW ratio, is depicted in Fig. 3(e). The incident beam divergences are calculated as full width at half maximum in the far field domain. As expected, the filtering performance depends on the distance between the diffraction grating and metamirror as well as on the initial beam. The numerical calculations show the maximal spectrum narrowing close to the ideal value of 0.5, i.e., the improvement of the beam quality factor M^2, by factor of 2.

Finally, full FDTD numeric simulations lead to analytically predicted results. In this case, we do not use the supercell approach but consider a broad integration area and simulate the reflection of an incident Gaussian beam of several different

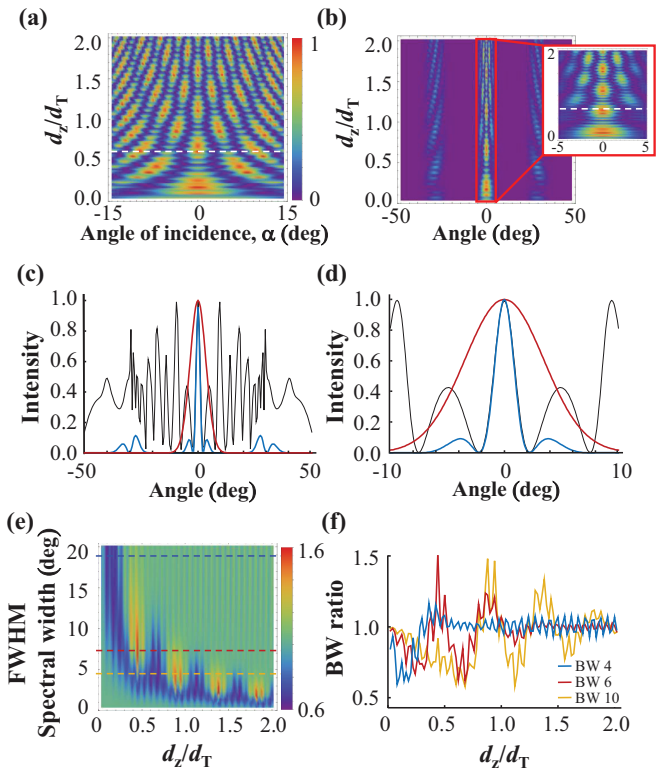

FIG. 3. Filtering performance. (a) Central mode reflectance map for a grating of rectangles with thickness of 0.7 μm, refractive index $n_2 = 1.68$, transverse period of $d_x = 2$ μm and 1 μm distance between rectangles. The dashed white line indicates the transverse cross-section at $d_z = 0.6d_T$ depicted in (c). (b) Three mode reflectance for the same structured-mirror for a Gaussian excitation at normal incidence, the inset shows a zoom-out. (c) Initial Gaussian 6-μm-wide beam profile (in red), reflectance profile (in black) and filtered beam profile (in blue) zoomed out in (d). (e) Map of divergence reduction. Ratio between reflected and incident angular widths, noted as BW ratio, as a function of the incident angular beam width (vertical axis) and grating-mirror separation (horizontal axis). (f) BW ratio as a function of mirror distance for three different values of the incident beam width: 4 μm (19° in blue), 6 μm (7.1° in red) and 10 μm (4.4°, in orange), highlighted in (e) by dashed horizontal lines.

divergence. We assume a structured metamirror composed from 61 elements, see Fig. 4(a). Figure 4(c) visualizes the angular narrowing effect of the spatial filtering. The angular cross section of the reflection of 10-μm-wide Gaussian beam exhibits a minimum for a metamirror configuration, corresponding to $d_z/d_T = 1.125$, as indicated by the white arrows in Fig. 4(c). A transverse cross section comparing both the incident and spatially filtered beam after reflection indicates a reduction of the beam quality factor M^2 down to 53%, see Fig. 4(d) in accordance with the analytical estimation. We finally analyze the angular divergence reduction as a function of the distance between the grating and the mirror, for three different incident beam widths, see Fig. 4(e). We find that the optimum filtering for broader spectra beams occurs at shorter distances between the grating and the mirror d_z as predicted by the general model [Figs. 3(e) and 3(f)].

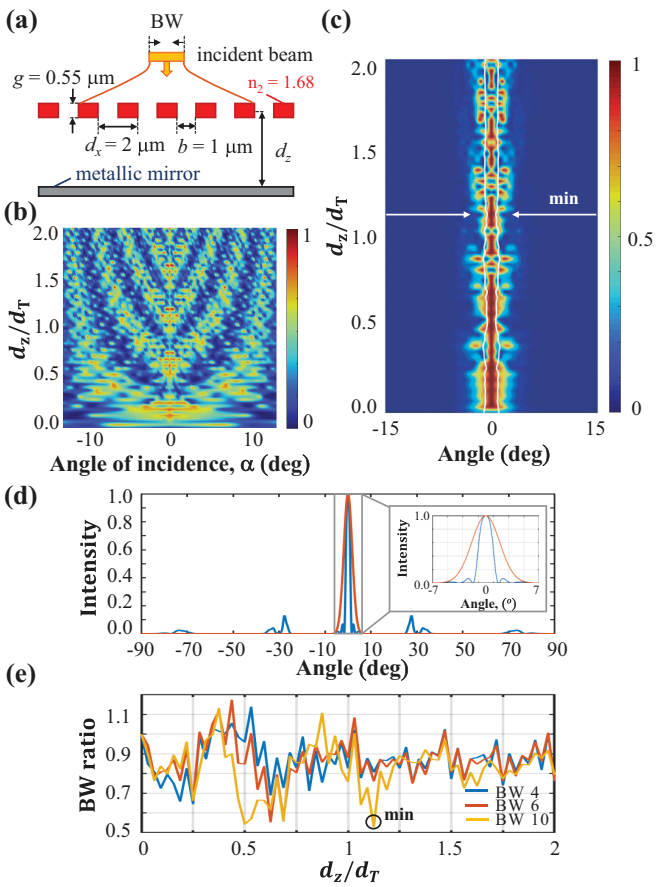

FIG. 4. Filtering performance. (a) Scheme of the full FDTD beam propagation simulations. A Gaussian beam is incident onto a grating of rectangular-shaped scattering objects (separated by $b = 1\ \mu$m, with thickness $g = 0.55\ \mu$m, refractive index, $n_2 = 1.68$) embedded in air ($n_1 = 1$) at a distance d_z from mirror. (b) 2D map of the zero-order plane wave reflection efficiency for different angles of incidence α, and the distance between the grating and the mirror, normalized to the Talbot distance, d_z/d_T, calculated using the supercell FDTD scheme. (c) 2D map of the far-field distribution for an incident Gaussian beam of 10-μm width. (d) Cross section of the far-field distributions for an incident Gaussian beam of 10 μm (in red) and reflected beam (in blue), for $d_z/d_T = 1.125$. (e) BW ratio when the width of the Gaussian beams is 4 μm (in blue), 6 μm (in red) and 10 μm (in orange), respectively.

V. CONCLUSIONS

In summary, we have proposed a 2D flat translationally-invariant, modulated mirror, and demonstrated its spatial filtering functionality. The arrangement consists of a periodic array of identical dielectric scattering objects in front of a highly reflecting mirror. The basic features of the proposed flat metamirror can be analytically described by a low contrast index model considering the grating and its mirror image (considering no back scattering). It is proven that transmission or reflection angular spectra depend on the periodical variation of the distance of the gratings to the mirror. The filter is also modeled by a high index scattering model that reveals the additional effects stemming from Mie and FP resonances. We have finally checked the results by precise FDTD numerical simulations. The filtering performance of the structured mirror shows a significant reduction of the beam quality parameter M^2 by a factor of 2 after reflection. The efficiency of the design could be increased by placing the structured mirror within a resonator, for example, a microlaser cavity.

ACKNOWLEDGMENTS

The authors acknowledge financial support from the Young Scholar Fellowship Program by the Ministry of Science and Technology (MOST) in Taiwan, under Grant No. MOST108-2636-M-027-002, also from NATO SPS research Grant No. 985048. K.S. acknowledges funding from European Social Fund (Project No. 09.3.3-LMT-K712-17-0016) under a grant agreement with the Research Council of Lithuania (LMTLT). K.S., R.H., and M.B. also acknowledge support by Spanish Ministerio de Ciencia e Innovación y European Union FEDER through Project No. PID2019-109175GB-C21.

APPENDIX A: FORWARD DIFFRACTION PARAXIAL MODEL

Here we discuss the derivation of the forward-diffraction paraxial model for a simple analytical study of the metamirror.

1. Scattering on a single diffraction grating

We expand the forward propagating field into three main components:$A(\vec{r}) = A_0 e^{i\vec{k}_0\cdot\vec{r}} + A_{-1} e^{i(\vec{k}_0-\vec{q})\cdot\vec{r}} + A_{+1} e^{i(\vec{k}_0+\vec{q})\cdot\vec{r}}$ for zero order $\vec{k}_0$ and first order $\vec{k}_0 \pm \vec{q}$ diffraction components. For convenience we write the field components in the form of a column-vector $\vec{A} = (A_{-1}, A_0, A_{+1})^T$ (T means transpose). The diffractive coupling among the components in propagation along z (cross the harmonic grating, with the diffractive spreading neglected) is given by

$$\vec{A}_z = \hat{M}\vec{A}, \tag{A1}$$

with the coupling matrix:

$$\hat{M} = \begin{bmatrix} 0 & im & 0 \\ im & 0 & im \\ 0 & im & 0 \end{bmatrix}, \tag{A2}$$

where $m = k\Delta n_0/(4n_0)$, and $k = n_0\omega/c$. The index modulation along the grating (transversally to the light propagation direction z) is assumed to be $n(x) = n_0 + (\Delta n_0/2)\cos(q_x)$.

The formal solution of the propagation equation is $\vec{A}(z)$ as shown in

$$\vec{A}(z) = \vec{A}(0)\exp(\hat{M}z). \tag{A3}$$

The calculation of the matrix (A2) exponent leads to $\hat{S} = \exp(\hat{M}d_z)$, denoted as

$$\hat{S} = \exp(\hat{M}d_z) = \begin{bmatrix} \frac{\cos(\sqrt{2}s)+1}{2} & \frac{i\sin(\sqrt{2}s)}{\sqrt{2}} & \frac{\cos(\sqrt{2}s)-1}{2} \\ \frac{i\sin(\sqrt{2}s)}{\sqrt{2}} & \cos(\sqrt{2}s) & \frac{i\sin(\sqrt{2}s)}{\sqrt{2}} \\ \frac{\cos(\sqrt{2}s)-1}{2} & \frac{i\sin(\sqrt{2}s)}{\sqrt{2}} & \frac{\cos(\sqrt{2}s)+1}{2} \end{bmatrix}. \tag{A4}$$

Here, $s = md_z = d_z\Delta n_0 k/(4n_0)$ in the limit of $s \ll 1$ (weak diffraction) has a meaning of linear scattering into diffraction modes, in terms of the field amplitude. This is easy

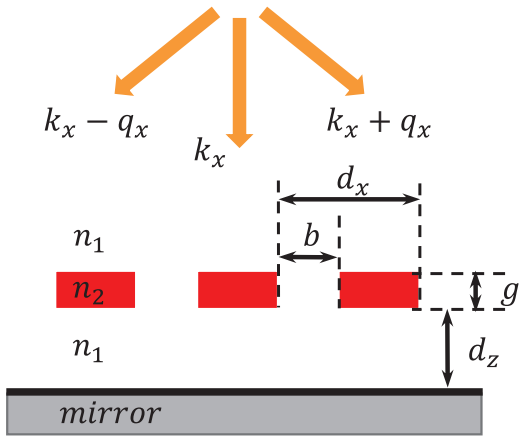

FIG. 5. Structured translationally-invariant metamirror composed by a grating of period d_x, consisting of rectangle elements with refractive index n_2 and thickness g, embedded in a medium with refractive index n_1, and separated at a distance d_z from a totally reflecting mirror.

to see from the series expansion of (A4), and noted as

$$\hat{S} = \begin{bmatrix} 1 - s^2/2 + \ldots & is - is^3/3 + \ldots & -s^2/2 + \ldots \\ is - is^3/3 + \ldots & 1 - s^2 & is - is^3/3 + \ldots \\ -s^2/2 + \ldots & is - is^3/3 + \ldots & 1 - s^2/2 + \ldots \end{bmatrix}, \tag{A5}$$

where increasing orders of scattering appear consecutively in the expansion. The scattering between modes first increase linearly with increasing s, however saturate and lead to periodic revivals for larger s (Rabi-Laue oscillations).

The matrix $\hat{S}$ is unitary: $\hat{S}\hat{S}^{T*} = \hat{I}$ where it means transposed and complex conjugated, and $\hat{I}$ is the identity matrix, which means that the field transformation conserves the energy $E = \vec{A}^{T*} \cdot \vec{A}$.

2. Free propagation between two gratings

The free propagation directly follows from the solution of the paraxial propagation equation:

$$A_z(x, z) = \frac{i}{2k}\nabla^2 A(x, z). \tag{A6}$$

The expansion of the field into harmonic components lead straightforwardly to the transformation after propagation over the distance z through diagonal propagation matrix:

$$\hat{P} = \mathrm{diag}\left(e^{\frac{-i(k_x-q_x)^2 d_z}{k_0}}, e^{\frac{-ik_x^2 d_z}{k_0}}, e^{\frac{-i(k_x+q_x)^2 d_z}{k_0}}\right), \tag{A7}$$

where $\vec{k}_x$ and $\vec{k}_x \pm \vec{q}_x$ are the transverse components of the zero and first diffraction order harmonics.

APPENDIX B: SEMIANALYTIC MODEL OF THE METAMIRROR

We model the structured metamirror as an array of rectangular elements in front of a flat, totally reflecting mirror, forming a FP cavity of thickness d_z, see Fig. 5.

The grating composed by rectangles of thickness g and refractive index n_2 embedded in a medium with refractive index n_1, can be considered as a pair of shifted diffraction gratings with period d_x. One grating consists of the rectangular elements of width $d_x - b$, each one considered as a Fabry-Perot cavity with refractive index n_2, thickness g and reflectivity in interfaces given by Fresnel equations. The second grating consists of the slits of width b between the rectangular elements.

The model considers the same three principal diffraction components of Appendix A written in vector form as $\vec{A} = (A_{-1}, A_0, A_{+1})^T$ for an incident wave vector $\vec{k}_0 = (k_x, k_z)$. The field reflected from the grating mirror composite is

$$\vec{A}_{\mathrm{ref}}(k_x) = [\hat{R} + \hat{T}\hat{P}\hat{R}_M(\hat{I} - \hat{R}\hat{P}\hat{R}_M)^{-1}\hat{T}]\vec{A}_{in}, \tag{B1}$$

where $\hat{I}$ is the identity matrix, The reflection matrix $\hat{R}$ and transmission matrix $\hat{T}$ of the grating are

$$R_{lj} = (-1)^{j-l}(d_x - b) \times \mathrm{sinc}((j-l)(d_x - b)\pi/d_x)\, r_{\mathrm{rec}}(k_x + jq_x) \tag{B2}$$

and

$$T_{lj} = be^{-i\psi(k_x+jq_x)}\mathrm{sinc}((j-l)b\pi/d_x) + (-1)^{j-l}(d_x - b)\mathrm{sinc}((j-l)(d_x - b)\pi/d_x) \times t_{rec}(k_x + jq_x) \tag{B3}$$

with subindexes $j, l = -1, 0, 1$, respectively.

The phase-shift in propagation through the slits between rectangles $\psi(k_x)$ is given as

$$\psi(k_x) = k_0 g n_1 \sqrt{1 - (k_x/k_0)^2}. \tag{B4}$$

The reflection and transmission coefficients r_{rec} and t_{rec} of the rectangular elements given by the Fabry-Perot cavity are

$$r_{rec}(k_x) = \frac{r(k_x)(1 - e^{-i\varphi(k_x)})}{(1 - r^2(k_x)e^{-i\varphi(k_x)})} \tag{B5}$$

and

$$t_{rec}(k_x) = \frac{(1 - r^2(k_x))}{(1 - r^2(k_x)e^{-i\varphi(k_x)})}, \tag{B6}$$

where the cavity phase-shift is $\varphi(k_x)$

$$\varphi(k_x) = 2gk_0\sqrt{n_2^2 - n_1^2(k_x/k_0)^2}, \tag{B7}$$

and the interface reflection for perpendicularly polarized light is given by the Fresnel equations

$$r(k_x) = \frac{n_1\sqrt{k_0^2 - k_x^2} - n_2\sqrt{k_0^2 - (n_1 k_x/n_2)^2}}{n_1\sqrt{k_0^2 - k_x^2} + n_2\sqrt{k_0^2 - (n_1 k_x/n_2)^2}}. \tag{B8}$$

The totally reflecting mirror is modeled by the matrix $\hat{R}_M = -\hat{I}$ for a metallic mirror, and $\hat{R}_M = \hat{I}$ for a dielectric mirror.

Finally, the light propagation between the structured layer and mirror is modeled by the propagation $\hat{P}$ matrix with elements:$P_{lj} = \exp(i2d_z n_1\sqrt{k_0^2 - (k_x + jq)^2})$ for $l = j$ and $P_{lj} = 0$ for $l \neq j$.

[1] S. Takimoto, T. Tachikawa, R. Shogenji, and J. Ohtsubo, IEEE Photon. Technol. Lett. **21**, 1051 (2009).
[2] J. Martín-Regalado, G. H. M. van Tartwijk, S. Balle, and M. San Miguel, Phys. Rev. A **54**, 5386 (1996).
[3] J. Li, K. Ueda, L. Zhong, M. Musha, A. Shirakawa, and T. Sato, Opt. Express **16**, 10841 (2008); **16**, 10848 (2008).
[4] S. K. Mandre, I. Fischer, and W. Elssser, Opt. Lett. **28**, 1135 (2003); **28**, 1137 (2003).
[5] K. Staliunas and V. J. Sánchez-Morcillo, Phys. Rev. A **79**, 053807 (2009).
[6] E. Colak, A. O. Cakmak, A.E. Serebryannikov, and E. Ozbay, J. Appl. Phys. **108**, 113106 (2010).
[7] Z. Luo, Z. Tang, Y. Xiang, H. Luo, and S. Wen, Appl. Phys. B **94**, 641 (2009).
[8] L. Maigyte, T. Gertus, M. Peckus, J. Trull, C. Cojocaru, V. Sirutkaitis, and K. Staliunas, Phys. Rev. A **82**, 043819 (2010).
[9] V. Purlys, L. Maigyte, D. Gailevičius, M. Peckus, M. Malinauskas, and K. Staliunas, Phys. Rev. A **87**, 033805 (2013).
[10] L. Maigyte and K. Staliunas, Appl. Phys. Rev. **2**, 011102 (2015).
[11] A. E. Serebryannikov, P. Lalanne, A. Y. Petrov, and E. Ozbay, Opt. Lett. **39**, 6193 (2014).
[12] A. E. Serebryannikov, A. Lakhtakia, M. Aalizadeh, E. Ozbay, and G. A. E. Vandenbosch, Sci. Rep. **8**, 15044 (2018).
[13] A. E. Serebryannikov, A. Y. Petrov, and E. Ozbay, Appl. Phys. Lett. **94**, 181101, (2009).
[14] D. Gailevičius, V. Koliadenko, V. Purlys, M. Peckus, V. Taranenko, and K. Staliunas, Sci. Rep. **6**, 34173 (2016).
[15] S. Gawali, D. Gailevičius, G. Garre-Werner, V. Purlys, C. Cojocaru, J. Trull, J. Montiel, and K. Staliunas, Appl. Phys. Lett. **115**, 141104 (2019).
[16] V. Purlys, L. Maigyte, D. Gailevičius, M. Peckus, R. Gadonas, and K. Staliunas, Appl. Phys. Lett. **104**, 221108 (2014).
[17] L. Grinevičiūtė, C. Babayigit, D. Gailevičius, E. Bor, M. Turduev, V. Purlys, T. Tolenis, H. Kurt, and K. Staliunas, Appl. Surf. Sci. **481**, 353 (2019).
[18] G. D. Marshall, M. Ams, and M. J. Withford, in *Proceedings of the International Conference on Photonics Europe*, edited by G. C. Righini (SPIE, Strasbourg, 2006), p. 195–203.
[19] M. Malinauskas, A. Žukauskas, S. Hasegawa, Y. Hayasaki, V. Mizeikis, R. Buividas, and S. Juodkazis, Light Sci. Appl. **5**, e16133 (2016).
[20] M. Campbell, D. N. Sharp, M. T. Harrison, R. G. Denning, and A. J. Turberfield, Nature (London) **404**, 53 (2000).
[21] C. K. Ullal, M. Maldovan, E. L. Thomas, G. Chen, Y. J. Han, and S. Yang, Appl. Phys. Lett. **84**, 5434 (2004).
[22] R. Rabady and I. Avrutsky, Opt. Lett. **29**, 605 (2004).
[23] A. L. Fehrembach, A. Talneau, O. Boyko, F. Lemarchand, and A. Sentenac, Opt. Lett. **32**, 2269 (2007).